Improved Models for Predicting Bubble Velocity, Bubble Frequency and Bed Expansion in a Bubbling Fluidized Bed

*Cornelius Emeka Agu, Lars-Andre Tokheim, Marianne Eikeland and Britt M.E. Moldestad

Department of Process, Energy and Environmental Technology, University of South-Eastern Norway, 3918 Porsgrunn, Norway

**cornelius.e.agu@usn.no; Lars.A.Tokheim@usn.no; Marianne.Eikeland@usn.no; britt.moldestad@usn.no*

Abstract

An efficient design and operational control of a fluidized bed reactor often relies on accurate prediction of bubble properties. This paper employs measurement of bed void fraction in determining the bubble velocity in a given bed. An analytical model is developed for bubble rise velocity, which shows that the rise velocity of a single bubble is proportional to the rate of change of the bubble-projected area. Based on the model for bubble rise velocity, a correlation for bubble velocity is obtained as given by $\boldsymbol{u_b = \varphi_N(U_0 - U_{mf}) + 12.51\varphi_D(U_0 - U_{mf})^{0.362} d_b^{0.52}}$. Bubble frequency is also modelled and presented as $\boldsymbol{f_b = \left(0.52\left(\frac{d_b}{D}\right)^{1.48} + mu_b^n d_b\right)^{-1}}$, and bed expansion due to bubble flow in a larger particle bed ($Ar \geq 400$) is modelled by $\boldsymbol{\Delta e = \left[1 - 0.0873(U_0 - U_{mf})^{-0.362}\left(\frac{U_0}{D}\right)^{0.66}\left(1 - \gamma\left(\frac{U_0}{U_{mf}}\right)^{\beta-1}\right)^{0.66}\right]^{-1} - 1}$. The three models have been validated against experimental data and the results show that the bubble velocity model has a better prediction accuracy than the existing models for Geldart B and D particles with prediction errors of 15.5% and 12.0%, respectively. The results also show that the proposed bed expansion model predicts better than the existing models in the literature.

Keywords: Bubble velocity; Bed expansion; Bubble frequency; Fluidized bed; Slug rise velocity

1 Introduction

In bubbling fluidized bed reactors, the diameter and rise velocity of bubbles can be used to obtain the bed expansion, which helps in determining the reactor effective volume and residence time. In addition to reactor design, the bubble properties at a given gas velocity are also used to characterize bubbling behaviour in fluidized beds. This paper is aimed at presenting a set of models that can be used to predict bubble velocity and bubble frequency in a fluidized bed for a wide range of particle and bed properties, and also a model for predicting the overall bed expansion in a bubbling fluidized bed regime.

There are different correlations for predicting bubble velocity in the literature [1] but their prediction accuracies vary from one system to another. However, no available literature clearly presents a model for obtaining the bubble frequency. In the slugging regime, few correlations are available [2,3]. The available models for the slug frequency are correlations assuming a fully developed slug where the slug size is closer to the bed diameter. The slug frequency models may also be limited to a large particle (or rough small particle) bed since bubbles in such a bed can easily grow to the size of the bed diameter [4]. For a bed of small spherical particles, a slug may have a fully developed size far less than the bed diameter even at a very high gas velocity. For the bed expansion, the prediction is generally based on the two-phase theory, where it is assumed that the bed void fraction is a linear combination of bubble volume fraction and gas volume fraction in the emulsion phase of the bed [4]. The bed expansion obtained based on this theory depends on the bubble velocity and bubble volumetric flow rate, the accurate predictions of which have been a challenge. The bubble volumetric flow rate is usually obtained based on the two-phase theory [5], although there are other types of models [6,7] accounting for the shortcomings of this theory. Based on the form of modified two-phase theory proposed by Grace and Cliff [7], Agu et al. [8] proposed a model for predicting the bubble volumetric flux, which depends on the particle properties

including the sphericity. However, different models [9, 10, 11] are also available for the bed expansion in a fluidized bed.

To characterize a fluidized bed behaviour, different measurement techniques are used. These techniques include the invasive probe technique [12, 13] and the non-invasive tomographic technique [14, 15, 16, 17, 18]. For measurement of bubble velocity, two measurement sensors separated at a fixed position are often used. The time taken by a bubble to pass from the lower to the upper sensor is obtained using a reconstruction technique such as the cross-correlation technique. One difficulty in this measurement method is identifying a single bubble as it rises across the two sensors. Near the distributor or when the gas velocity is very low, a large number of bubbles is often present, making it difficult to identify which bubble that passes the measurement sensors at a given time. Depending on the spacing between the sensors, the shape and size of the bubble may also change before reaching the upper sensor due to coalescence or splitting of the bubble. Moreover, the bubble velocity obtained using this method is an average value within a section of the bed. The minimum spacing required between two sensors to avoid signal interference makes it difficult to measure the absolute local bubble velocity. This paper employs the measurement of bubble volumetric flow rate and bubble volume fraction to determine the local bubble rise velocity. The bubble volume fraction is calculated from the two-phase theory assuming that the emulsion-phase voidage is the same as the local bed void fraction at the minimum fluidization condition. Using a two-plane ECT (electrical capacitance tomography) sensor, the local bed void fraction for a given gas velocity is measured at different locations in the bed. From the analysis of the changes in the projected area of a spherical bubble, a model for bubble rise velocity is developed. The model coefficient is obtained by fitting the analytical bubble velocity with the measured bubble velocity. In the subsequent sections, a model for predicting the bubble frequency

based on the local bubble velocity is developed, and finally an expression for predicting bed expansion in the bubbling regime is developed. The results are presented and discussed.

2 Analysis of bubble flow

In a bubbling fluidized bed, bubble velocity u_b is generally given as in Eq. (1), following some modifications of the Davidson and Harrison [19] model.

$$u_b = \emptyset\left(U_0 - U_{mf}\right) + u_{br} \tag{1}$$

$$u_{br} = \alpha\sqrt{g d_b} \tag{2}$$

Here, U_0 is the superficial gas velocity, U_{mf} is the minimum fluidization velocity of the bed material and u_{br} is the bubble rise velocity. The coefficient $\emptyset$ accounts for presence of more than one bubble and their effect on the rising of an individual bubble [4]. The coefficient α in Eq. (2) accounts for possible wall effects on the rising of a single bubble, whereas g and d_b are the gravity constant and the bubble diameter, respectively. There are different values for α being used [19, 20, 21, 22] depending mainly on the particle size (solids classification according to Geldart [23]). In addition to Eq. (1), other models for bubble velocity are also available [21, 24]. This section introduces a new model for bubble rise velocity and a model for bubble frequency.

For a single bubble rising through a fluidized bed, a typical time variation of its projected area is shown in Fig. 1(a). The bubble-projected area at a given time is shown in Fig. 1(b). Fig. 1(a) shows that when one bubble passes through a plane, there is a time lag before another one can be observed. The time frame between when a bubble arrives and when it completely leaves a plane is described as the active period, T_{ba}. The time between arrivals of two successive bubbles to the fixed plane is the bubble period, T_b, and the time at which the plane is free of bubbles is the bed idle period, T_i.

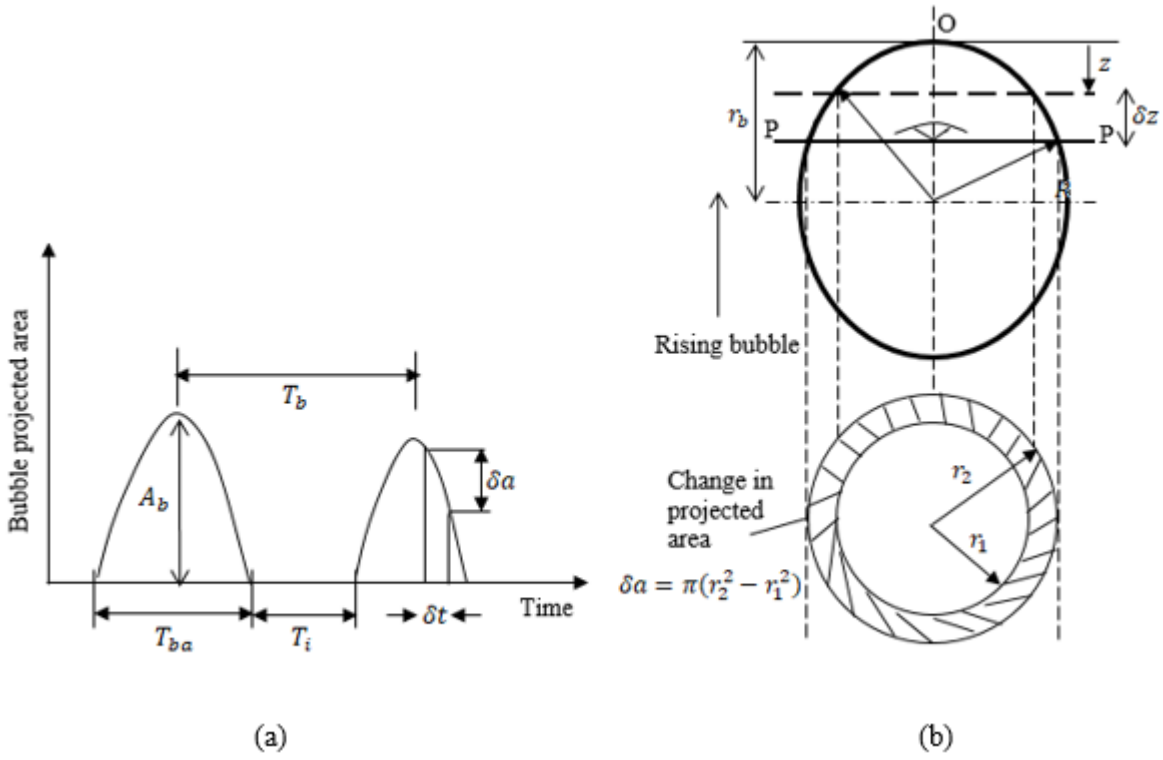

Fig. 1. Variation of bubble-projected area (a) evolution with time (b) changes with vertical axis.

2.1 Bubble rise velocity

Considering an isolated wakeless spherical bubble rising through a fluidized bed, different cross-sectional areas (projected areas) can be observed at different times at the plane P-P. As shown in Fig. 1, the bubble-projected area changes from $a_1 = \pi r_1^2$ to $a_2 = \pi r_2^2$ as the bubble rises through a vertical distance δz within a time interval δt.

By geometry, the radii r_1 and r_2 can be related to the bubble radius $r_b = d_b/2$, when $z < r_b$, by

$$r_1^2 = z(2r_b - z) \tag{3}$$

$$r_2^2 = (z + \delta z)[2r_b - (z + \delta z)] \tag{4}$$

Multiplying both sides of Eqs. (3) and (4) by π and taking the difference of the resulting equations, the change in the bubble projected area $\delta a = \pi(r_2^2 - r_1^2)$ is then expressed after simplification as

$$\delta a = \pi(2r_b - 2z - \delta z)\delta z \tag{5}$$

Dividing Eq. (5) through by δt, the change in the value of a for a small change in time becomes

$$\frac{\delta a}{\delta t} = \pi(2r_b - 2z - \delta z)\frac{\delta z}{\delta t} \tag{6}$$

For the limit when $\delta t \to 0$, $\delta z \to 0$. Then, Eq. (6) becomes

$$\frac{da}{dt} = \pi(2r_b - 2z)\frac{dz}{dt} \tag{7}$$

In Eq. (7), the rate of change of the vertical displacement z is the bubble rise velocity, thus $u_{br} = \frac{dz}{dt}$.

$$\frac{da}{dt} = \pi(2r_b - 2z)u_{br} \tag{8}$$

Dividing through by the bed cross-sectional area $A = \pi D^2/4$ to normalize Eq. (8).

$$\frac{1}{A}\frac{da}{dt} = \frac{4\pi(2r_b - 2z)}{\pi D}\frac{u_{br}}{D}$$

$$\frac{1}{4A}\frac{da}{dt} = \left(\frac{2r_b - 2z}{D}\right)\left(\frac{u_{br}}{D}\right) \tag{9}$$

Let $k = \frac{2(r_b - z)}{D}$, then

$$u_{br} = \left(\frac{D}{4Ak}\right)\frac{da}{dt} \tag{10}$$

For a given bed, Eq. (10) shows that the bubble rise velocity is proportional to the rate of change of the projected area with time. The value of the model parameter k depends on the

bubble diameter and time. Therefore, the time-averaged value of k for a given bubble will be required to obtain the velocity with which the bubble rises uniformly through a given plane in the bed. The variation of the average value of k with the flow condition can be determined from experiments. It should be noted that normalizing Eq. (8) with the bed cross sectional area makes the model constant k dimensionless. For this reason, the model in Eq. (10) can be used regardless of the bed diameter for which the k value was obtained.

Assuming that the time-variation of the bubble-projected area follows a parabolic function, $a = 4A_b(t/T_{ba} - (t/T_{ba})^2)$, it can be shown that $\left[\frac{da}{dt}\right]_{t=0} = \frac{4A_b}{T_{ba}}$ and $\left[\frac{da}{dt}\right]_{t=T_{ba}/2} = 0$. The average value of $\frac{da}{dt}$ is then

$$\frac{da}{dt} = \frac{2A_b}{T_{ba}} \tag{11}$$

where $A_b = \pi d_b^2/4$ is the bubble-projected area through its centre. The bubble properties T_{ba} and A_b can be measured in an experiment. The active bubble period strongly depends on the bubble diameter. The larger a bubble is, the longer it takes to pass through an observer plane. In Agu et al. [8], a correlation relating $1/T_{ba}$ with the bubble diameter d_b is proposed as described in Eq. (12), where the time is measured in seconds.

$$\frac{1}{T_{ba}} = 1.927\left(\frac{d_b}{D}\right)^{-1.48} \tag{12}$$

Combining Eq. (10), (11) and (12) yields

$$u_{br} = 1.927A_b\left(\frac{D}{2Ak}\right)\left(\frac{d_b}{D}\right)^{-1.48}$$

$$u_{br} = \frac{0.9635}{k}\left(\frac{d_b}{D}\right)^{2}\left(\frac{d_b}{D}\right)^{-1.48} D$$

$$u_{br} = \frac{0.9635}{k}\left(\frac{d_b}{D}\right)^{0.52} D \tag{13}$$

2.2 Bubble frequency

From Fig. 1(a), the total bubble period T_b can be expressed as

$$T_b = T_{ba} + T_i \tag{14}$$

The bubble frequency $f_b = 1/T_b$ can thus be obtained from

$$f_b = 1/(T_{ba} + T_i)$$

Substituting Eq. (12) in the above equation yields

$$f_b = \left(0.52\left(\frac{d_b}{D}\right)^{1.48} + T_i\right)^{-1} \tag{15}$$

The bed idle period T_i depends on the bubble rise velocity. The faster the bubbles rise, the more active the bed is, thus the lower the idle period. Since T_i can be measured in any given bed, its relationship with the bubble velocity can be obtained from experimental data.

3 Set up and measurement procedure

The experimental set up consists of a 10.4 cm cylindrical column of height 1.4 m. The column is fitted with a porous plate and a set of two-plane ECT sensors separated at a distance of 13 cm. Here, only a brief description of the experimental set up is given. The details of this set up, the materials used and the operating conditions have previously been described in [8, 22], hence will not be repeated. The method used to obtain the relevant bubble properties are also outlined in the previous studies.

The experiments were conducted at ambient conditions using air as the fluidizing gas. Six different types of particles with mean particle size in the range of 180 – 2200 μm were used. For each of these powders given in Table 1, the particle size, $d_p$was obtained from sieve analysis and particle density, ρ_p with a gas pycnometer. A bed of each particle type was formed in the fluidized bed column with initial bed height within 40 – 60 cm to ensure that

both ECT sensors were covered by the particles. The experiment was repeated five times at each air velocity for a given bed. The image data recorded by the ECT sensors were captured at a frequency of 100 Hz for 60 s.

The ECT data provide information about the distribution of solids or void at the sensor position. The average void fraction and the standard deviation were computed as discussed in Agu et al. [25]. The standard deviation plot against the gas velocity was used to determine the minimum fluidization and slugging velocities , U_{mf} and U_{ms}, respectively. The ECT data were also analysed to identify bubbles, their properties and their behaviour over the measurement period [8, 25]. To verify the repeatability of the experiment, the five data sets for each gas velocity were analysed separately, and the mean variation in the measurements when the experiment is repeated was observed to be less than 2.5%. The average data from the five measurements was therefore taken to reduce random errors.

Table 1. Bed materials investigated with properties.

Materials	Geldart type	Shape	$\boldsymbol{\rho_p}$ [kg/m^3]	$\boldsymbol{d_p}$ [µm]	$\boldsymbol{U_{mf}}$ [cm/s]	$\boldsymbol{U_{ms}}$ [cm/s]
Glass	B	spherical	2500	188	3.80	14.50
Glass	B	spherical	2500	261	8.15	14.69
Glass	B	spherical	2500	624	23.20	33.80
Limestone	B	angular	2837	293	13.80	21.16
Limestone	B/D	angular	2837	697	39.24	49.00
Sand	B	angular	2650	483	16.50	25.82
Molecular sieve	D	spherical	1300	2170	76.85	91.57

From the data analysis, it was observed that the growth of a bubble as gas velocity is increased depends on the particles. With increase in particle size, the bubble growth rate increases. In the bed of angular (rough) particles, the rate of bubble growth is higher in the

lower part of the bed than in the upper section, resulting in a sharp transition from bubbling to slugging regime. Moreover, the slug flow in the bed of limestone particles changes from the flat slug type to wall slug type at a considerably high gas velocity, probably due to the cohesive nature of these particles. For the spherical (smooth) particles, the rate of bubble growth is almost uniform over the bed, and the transition from bubbling to slugging regime is smooth.

For further analysis, the bed behaviour observed in this study is classified into two types based on the bubble growth rate:

- Type A: Bed with a slow bubble growth rate and a smooth transition from bubbling to slugging regime. Slugs rise along the central axis with a full-grown size less than the bed diameter; this behaviour is typical for fine and smooth Geldart B particles.
- Type B: Bed with a rapid bubble growth rate or a sharp transition from bubbling to slugging regime. Slugs spread across the bed cross-section and attach to the wall while rising. Slugs can grow to the bed size; this behaviour is typical for large particles or rough smaller particles.

Moreover, the bubble growth rate depends on the bed height to diameter ratio. As all the beds studied are deep, it is further observed that rough particles with a mean diameter as large as 300 μm exhibit a type B behaviour. For a bed with type A behaviour, data analysis also shows that there is a retardation in the slug growth when the ratio of bubble diameter to bed diameter is between the value of $(d_b/D)_{fm}$ and 0.6. Here, $(d_b/D)_{fm}$ is the bubble diameter at which the bubble frequency is at its local maximum, and at which slugs begin to appear at the bed position. The subscript "fm" denotes maximum frequency. The value of $(d_b/D)_{fm}$ depends on the particles, and increases slightly along the bed height. The average value of $(d_b/D)_{fm}$ over a given bed is shown in Fig. 2(a) as a function of U_{ms}/U_{mf}. The figure shows that the

bubble diameter at the local maximum frequency increases with decreasing U_{ms}/U_{mf}, indicating that the $(d_b/D\,)_{fm}$ value increase with particle size. The curve correlating the measured $(d_b/D\,)_{fm}$ with U_{ms}/U_{mf} value in Fig. 2(a) can be represented by Eq. (16).

$$(d_b/D)_{fm} = \left(2.90 - 36.66\exp\left(-2.80\frac{U_{ms}}{U_{mf}}\right)\right)^{-1} \tag{16}$$

Fig. 2(b) shows the variation of $1/(v_b/T_i)$ with u_b, where v_b is the bubble volume and u_b is the bubble velocity obtained as described in the subsequent sections. The figure clearly shows the behaviour of a bed due to bubble growth. The T_i/v_b value is higher for type B than for type A behaviour at the same bubble velocity, indicating that the bubble frequency is lower in the bed of larger particles than in the bed of smaller particles for the same volume of bubbles. In addition, the slopes of the trend lines for the type B behaviour are higher than the corresponding slopes in the type A beds. That is, -6.9 and -1.7 for B1 and B2, and -5.8 and -1.2 for A1 and A2, respectively. This means that the response to changes in the bubble activities is higher in the bed of larger particles than in that of smaller particles for a unit change in the flow property (gas velocity or bubble velocity). As can also be seen, three different lines are associated with the type A behaviour, and this is due to the slug growth transition as explained above.

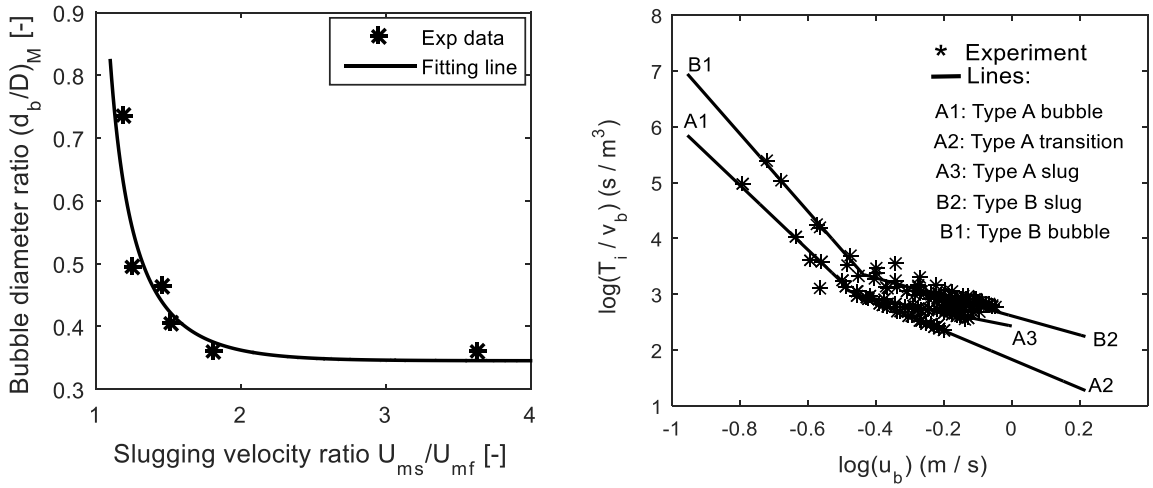

(a) (b)

Fig. 2. (a) variation of bubble diameter at maximum frequency with minimum slugging velocity ratio based on the three glass, two limestone and the molecular sieve particles given in Table 1. (b) Bed idle period per unit bubble volume for two different types of behaviour in a fluidized bed; data from the three glass and the sand particles in Table 1.

3.1 Measurement of bubble velocity

The bubble velocity at the two different positions in the bed is obtained based on the mass balance, where

$$u_b = G/\delta_b \tag{17}$$

Here, G is the volumetric bubble flux obtained as in Eq. (18).

$$G = \frac{\pi}{6AT_{ba}} d_b^3 \tag{18}$$

Based on the two-phase theory, the bubble volume fraction at each of the measurement positions is calculated from the following relationship (which is also based on the mass balance) [4]

$$\varepsilon_f = \delta_b + (1 - \delta_b)\varepsilon_{mf}$$

$$\delta_b = \frac{\varepsilon_f - \varepsilon_{mf}}{1 - \varepsilon_{mf}} \tag{19}$$

Here, ε_f is the local bed void fraction and ε_{mf} is the corresponding value at the minimum fluidization condition. In Eq. (19), the void fraction in the emulsion phase is assumed the same as ε_{mf} since the particles used in this study are considered to be in the Geldart B group [4]. It should be noted that Eq. (19) is valid only at low gas velocities. At a higher gas velocity, the void fraction in the emulsion phase is larger than ε_{mf} due to excessive bed expansion.

4 Model development and results

With measurement of relevant bubble properties, the complete models for the bubble velocity, bubble frequency and bed expansion can be derived. The accuracies of these models against experimental data are evaluated based on the mean absolute error.

4.1 Model for bubble rise velocity

As the bed under this study is deep, visual observation and data analysis reveal that only a single bubble rises through the bed within the range of gas velocity investigated, thus $\emptyset = 0$ and from Eq. (1), $u_{br} = u_b$. Using the measured bubble rise velocity $u_{br,exp}$, the model parameter k in Eq. (13) can be determined from

$$k = \frac{0.9635\left(\frac{d_b}{D}\right)^{0.52} D}{u_{br,exp}} \tag{20}$$

Fig. 3 shows the variation of k with excess gas velocity $U_0 - U_{mf}$ on the logarithmic scale. As shown in the figure, the model parameter decreases with increasing gas velocity. The line fitting the data in the figure is given by the equation

$$k = 0.077(U_0 - U_{mf})^{-0.362} \tag{21}$$

For the correlation in Eq. (21), the gas velocity $U_0 - U_{mf}$ is in **m/s**. Substituting Eq. (21) into Eq. (13) yields

$$\boldsymbol{u_{br} = 12.51(U_0 - U_{mf})^{0.362}\left(\frac{d_b}{D}\right)^{0.52} D} \tag{22}$$

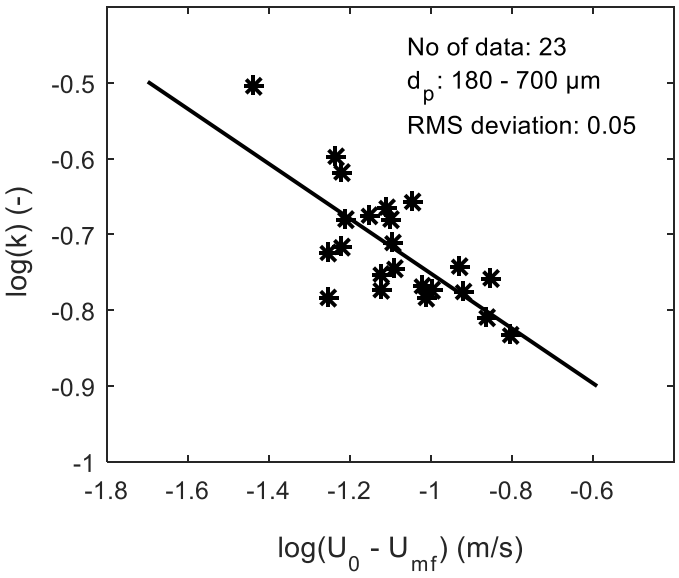

Fig. 3. Correlation for the model parameter k in Eq. (13).

Equation (22) shows that bubble rise velocity increases approximately with the square root of the bubble diameter, which is in agreement with Eq. (2). The variation of u_b with $D^{0.48}$ in Eq. (22) also agrees quite well with $D^{0.4}$ in the Werther [26] model and with $D^{0.5}$ in the Hilligardt and Werther [6] model for Geldart B particles. With the term $(U_0 - U_{mf})^{0.362}$, Eq. (22) can also predict an increase in the slug rise velocity with increasing gas velocity when the bubble diameter approaches a constant value. Generally, the available models for slug rise velocity, u_s are in the form

$$u_s = k_1\left(U_0 - U_{mf}\right) + k_2\sqrt{gD} \tag{23}$$

where $k_1 = 1.0$ is usually applied. The value of k_2 depends on the type of slug. For an axisymmetric slug, $k_2 = 0.35$ [27], and for a wall slug $k_2 = 0.35\sqrt{2}$ [28]. Both types of slug can also be present in a given bed depending on the particle properties and gas velocity. The term $(U_0 - U_{mf})^{0.362}$ also suggests that Eq. (22) is continuous and therefore can be applied for all values of $U_0 - U_{mf}$. It should be noted that the superficial gas velocity, U_0 has to be varied to achieve the same excess gas velocity, $U_0 - U_{mf}$ for different particles since U_{mf} can

vary from particles to particles. Moreover, since the model is continuous over the gas velocities, it can also be applied in the transition regime between bubbling and turbulent flow /slugging provided that the bubble diameters within these regimes are used. For example, bubble breaks to a lower size at the transition to turbulent flow regime, but grows towards the bed diameter as the bed transits into slugging regime. The maximum bubble diameter at the onset of transition into turbulent flow regime can be estimated as given in Bi [29] while the minimum bubble diameter at the transition into slugging regime can be estimated from Eq. (16).

Fig. 4 compares the bubble rise velocity predicted with the proposed model, Eq. (22) against the experimental data within the bubbling regime. The results are obtained at the position $h = 15.7$ cm above the distributor. The predictions obtained from some of the existing models are also shown including the slug rise velocity based on Eq. (23) for both values of k_2. As can be seen in both figures, Eq. (22) predicts the experimental data with a good accuracy. Both the Werther [26] and Hilligardt and Werther [6] models predict the bubble rise velocity with larger errors but the accuracy is better using the Hilligardt and Werther model as shown in Fig. 4. The Davidson and Harrison [19] model over predicts the bubble rise velocity in both beds although the agreement is better for the 697 μm limestone particles. In addition, the results show that the Werther [26] model and the Davidson and Harrison [19] model do not predict the velocity of the rising slug when the bubble/slug diameter approaches a constant value. The Hilligardt and Werther model predicts the slug rise velocity in agreement with Eq. (23) when $k_2 = 0.35$ as can be seen in Fig. 4(b). However, in comparison with the proposed model, the Hilligardt and Werther model under predicts the slug velocity in both beds, although the model prediction is closer to the result from the 261 μm particle bed since the rising slug is of axisymmetric type. Comparing with Eq. (23), the results in Fig. 4 also show that the proposed

model predicts accurately the slug rise velocity in accordance with the two different types of slug.

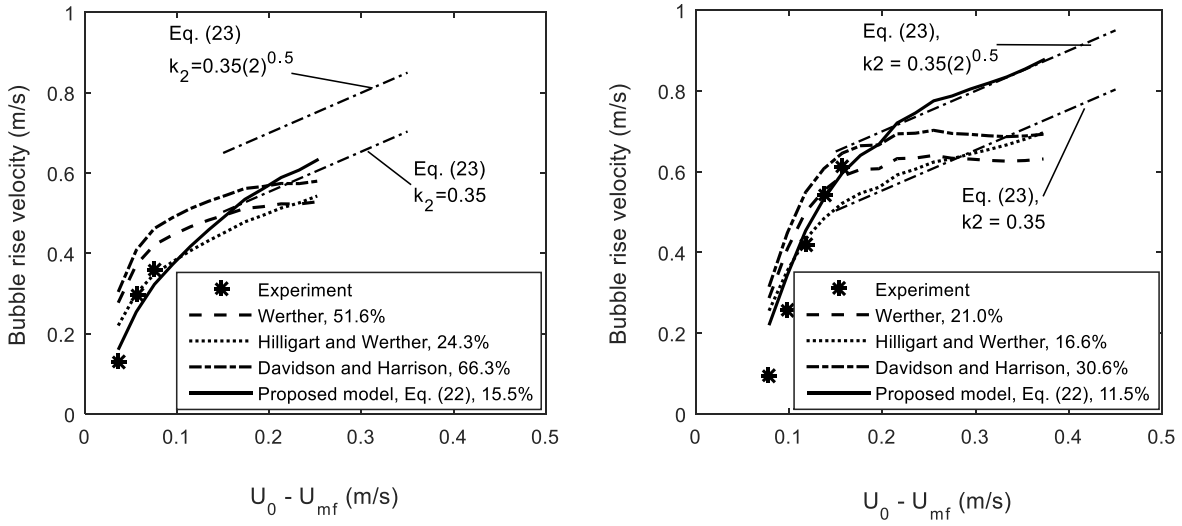

(a) (b)

Fig. 4. Variation of bubble rise velocity with excess gas velocity predicted based on Eq. (22) compared with experimental data and other models for two different beds (a) 261 μm glass particles (b) 697 μm limestone particles.

4.2 Model for bubble velocity

Although the model parameter given by Eq. (21) is obtained from a bed containing single bubbles, Eq. (22) can also be applied in a bed with more than one bubble rising across any plane in the bed. In this case, the rise velocity of each bubble can be obtained from Eq. (22), with d_b the same as the average diameter of all the bubbles present in the bed position. The bubble velocity u_b due to flow of these bubbles can then be determined by adding the flux term, $\emptyset\left(U_0 - U_{mf}\right)$ as described in Eq. (1). When the bubbles coalesce into a single bubble, this flux term can be neglected since a higher bubble diameter (equivalent to volume of all the bubbles) is then used in Eq. (22).

A comparison with published experimental data [6, 30] shows that the proposed model given by Eq. (22) for bubble rise velocity is sufficiently accurate for predicting the bubble velocity. For Geldart A particles, the experimental bubble velocity given by Hilligardt and Werther [6] at different bed diameters and gas velocities can be predicted with a good accuracy when Eq. (22) is substituted for u_{br} in Eq. (1) for which $\emptyset = 1$. The value of $\emptyset$ is unity in this group of particles since more than a bubble may be present due to low bubble coalescence [4]. For the data presented in [6] for Geldart B solids ($U_{mf} = 0.18$ m/s), Eq. (22) predicts the bubble velocity accurately with $\emptyset = 0$, which is similar to the case in this study for particles belonging to the same Geldart group. In a 1.2 m diameter bed of sand particles with a mean size of 1.0 mm, Glicksman et al. [30] presented data for bubble velocity at different superficial gas velocities. Comparing the predictions from Eq. (22) with these data when $\emptyset = 0$, it can be observed that the model also accurately predicts the experimental data if 60% of the bed diameter in this current study is used. This reduced bed diameter also fits the model accurately to the data obtained in this study for the 2.17 mm molecular sieve particles. Based on these results, the following model is proposed for bubble velocity in a fluidized bed.

$$\boldsymbol{u_b = \varphi_N\left(U_0 - U_{mf}\right) + 12.51\varphi_D(U_0 - U_{mf})^{0.362} d_b^{\,0.52}} \tag{24}$$

where

$$\varphi_N = \begin{cases} 1 & \text{for Geldart A and A/B} \\ 0 & \text{for Geldart B and D} \end{cases} \tag{25}$$

$$\varphi_D = \begin{cases} D^{0.48} & \text{for type A behaviour (Geldart A and small Geldart B particles)} \\ 0.337 & \text{for type B behaviour (large Geldart B particles)} \\ 0.26 & \text{for Geldart D} \end{cases} \tag{26}$$

As demonstrated in Fig. 4, Eq. (24) can also be used to predict the slug rising velocity in a fluidized bed. For example, in a cylindrical bed of diameter 76.2 mm, the slug velocity

reported in Wang et al. [14] for spherical iron oxide particles (mean particle size 1.5 mm) can be predicted with good accuracy using Eq. (24), where $\varphi_N = 0$ and $\varphi_D = 0.26$.

For further demonstration, the predictions of the proposed model, Eq. (24) are compared with those of the existing models [6, 19, 26] in Fig. 5. The existing models given by Davidson and Harrison [19], Werther [26] and Hilligardt and Werther [6] are widely used in fluidized bed studies. The experimental data are based on those obtained in this study for Geldart B and D particles, those given in Hilligardt and Werther [6] for Geldart A and B particles, and on those given in Glicksman et al. [30] for D particles. Fig. 5(a) shows that the Werther model as well as the Hilligardt and Werther model have high accuracies in predicting the experimental data. The mean error associated with the model prediction for the Geldart A particle are 7.2 and 8.5%, respectively. The prediction errors based on these two models increases with increase in the gas velocity and can be over 12.0% according to the data in Fig. 5(a). The Davidson and Harrison model under predicts the experimental data with a mean error of 54.3% while the proposed model under predicts the bubble velocity with error in the range of 17 – 50%. Although this range of error is too high for practical application, the accuracy of Eq. (24) for Geldart A particles increases with increase in the gas velocity or bed diameter. The 17% error in this range is obtained from those data associated with higher gas velocities and larger bed diameter while the 50% error is associated with data at lower gas velocity and smaller bed diameter. Since industrial operations based on Geldart A particles are at very high gas velocity compared to the particle minimum bubbling velocity, this shows that the proposed model will be suitable for large scale application.

Moreover, for the Geldart B and D particles, the proposed model has a better accuracy compared to the other models. The mean prediction error using Eq. (24) is 15.5% for the group B particles. The Werther model predicts the data for the particles in the Geldart B group with an error of 28.1%. The errors for predicting the group B data using the Hilligardt

and Werther model as well as the Davidson and Harrison model are 18.6 and 36.6%, respectively. For the Geldart D particles, these last two models also have a wide prediction error compared to the proposed model, which shows 12% error in predicting the experimental data. However, due to small number of data used in Fig. 5(c), the model comparison cannot be concluded in this study, and the comparison for the group A powder is not also exhaustive for the same reason. Since a large number of data set is shown for the group B powders, it can be concluded that for this group of particles, the accuracy of the proposed model is better than those of the previous models.

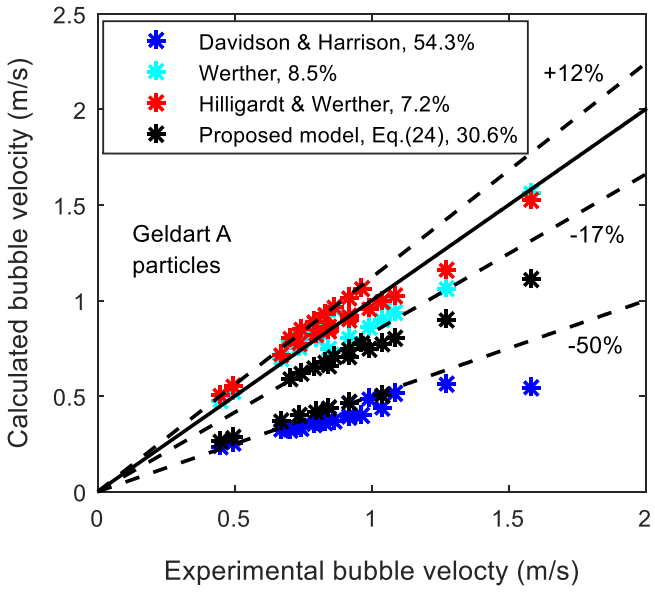

(a)

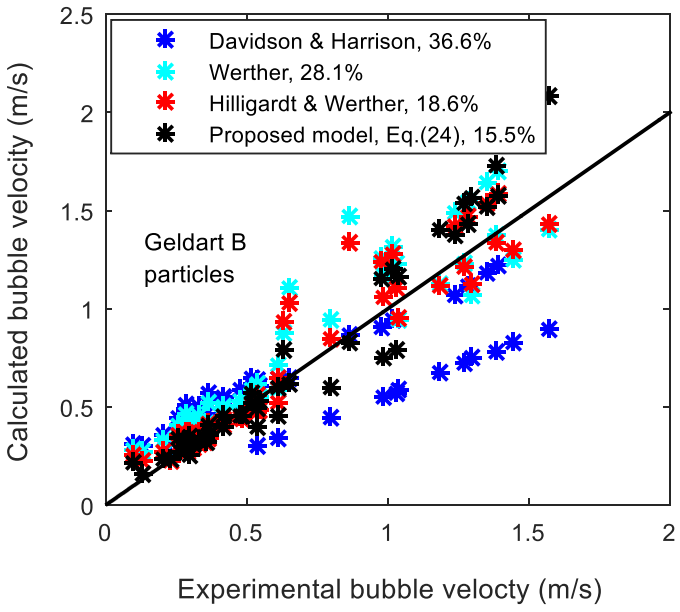

(b)

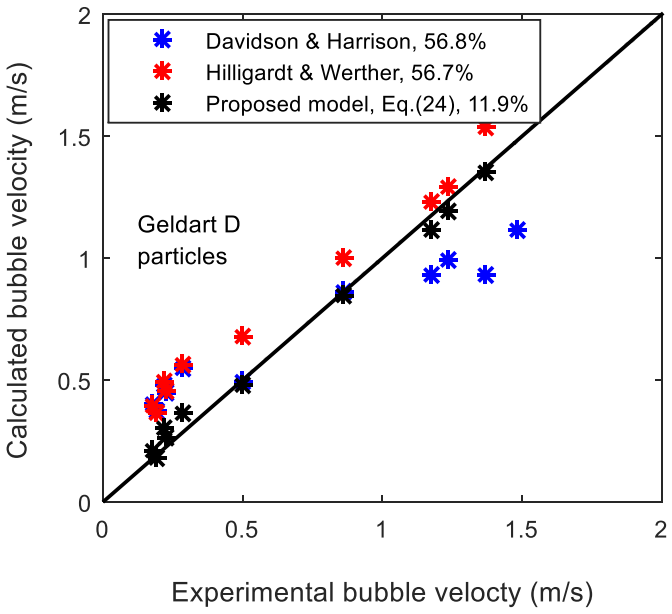

(c)

Fig. 5. Computed bubble velocity versus experimental data for different particle groups (a) Geldart A (b) Geldart B (c) Geldart D.

4.3 Model for bubble frequency

Bubble frequency depends on the bubble growth rate in a given bed. With reference to the rising of single bubbles in a fluidized bed, bubble frequency is defined as the number of such bubbles crossing a fixed plane per unit time. The larger the number of these bubbles, the higher is the bubble frequency. When a bubble grows to the size that slugs begin to appear, the bubble frequency decreases with further increase in the bubble size. For a given bubble diameter, a lower bubble/slug frequency indicates that the idle period of the bed is longer.

From analysis of the data given in Fig. 2, a correlation for the bed idle period T_i is obtained as given in Eq. (27).

$$T_i = m u_b^n d_b \tag{27}$$

Bubbling regime, $\frac{d_b}{D} \leq \left(\frac{d_b}{D}\right)_{fm}$: $\begin{cases} m = 0.05\,; n = -3.475 & \text{for type A} \\ m = 0.05\,; n = -4.379 & \text{for type B} \end{cases}$

Slugging regime, $\frac{d_b}{D} > \left(\frac{d_b}{D}\right)_{fm}$: $\begin{cases} m = 0.631\,; n = -1.187 & \text{for type A, } \frac{d_b}{D} \leq 0.6 \\ m = 3.382\,; n = -0.122 & \text{for type A, } \frac{d_b}{D} > 0.6 \\ m = 5.277\,; n = -0.366 & \text{for type B} \end{cases}$

Combining Eq. (27) with Eq. (15), the model for bubble frequency is therefore given by

$$\boldsymbol{f_b = \left(0.52\left(\frac{d_b}{D}\right)^{1.48} + m u_b^n d_b\right)^{-1}} \tag{28}$$

The predictions from Eq. (28) at different gas velocities for two different powders are shown in Fig. 6. As can be seen, the model results agree very well with the experimental data obtained in the bed of 188 μm glass particles. For the bed of sand particles, there is also good agreement between the model predictions and the experimental data. The results in the figures show that the model also captures the trend of the bubble frequency with varying gas velocity. The local maximum frequency is well predicted in both beds. For the results presented in the previous studies [31, 32], Eq. (28) can also be used to predict the bed behaviour. Eq. (28) can

predict with good accuracy for example, the axial distribution of the bubble frequency including the local peak value as reported in Weber and Mei [31] for a bed of 185 μm glass particles.

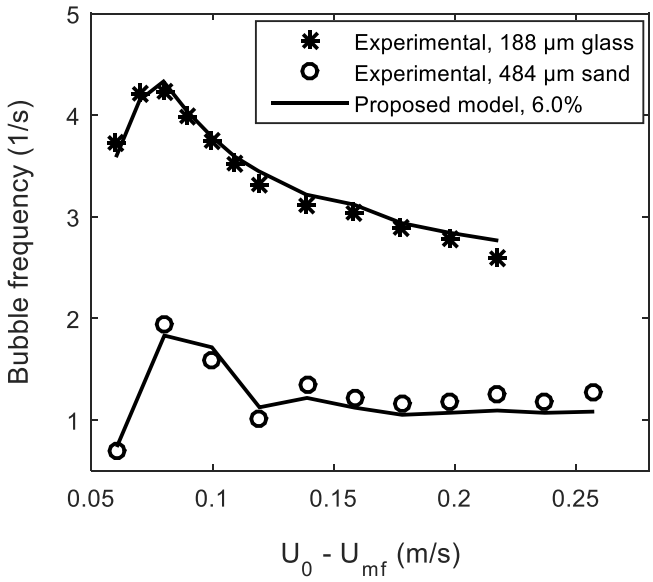

Fig. 6. Predicted bubble frequency using Eq. (28) compared with the experimental data at different gas velocities for the bed of 188 μm glass particles and 483 μm sand particles at $h = 15.7$ cm.

In addition, the overall prediction accuracy of Eq. (28) is shown in Fig. 7. The experimental data covers the range of powders used in this study. Similar to the results shown in Fig. 6, there is also a good agreement between the model predictions and the experimental data for the other powders. As shown in Fig. 7, the mean absolute error associated with the model prediction is 12.4%.

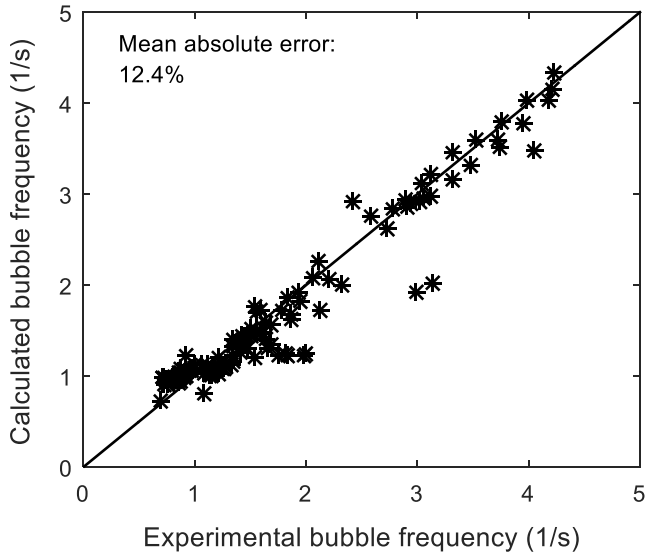

Fig. 7. Comparison of the computed results based on Eq. (28) with experimental results, showing the model accuracy based on the particles in Table 1.

With these results, the proposed model for bubble frequency can be used to predict the fluidized bed behaviour in both bubbling and slugging regimes. Moreover, Eq. (28) shows that when the bubble diameter is constant, the bubble frequency increases with the gas velocity. However, such a stable bubble diameter may be difficult to attain. As observed in this study, a slug splits once it reaches a size closer to the bed diameter. When a slug splits, the smaller slug rises with a lower velocity, thereby decreasing the slug frequency. This shows that the slug frequency may increase, decrease or remain constant when the slug diameter approaches the bed diameter depending on the net effect of slug splitting and coalescence. Hence, for accurate prediction of slug frequency using Eq. (28), measured bubble/slug diameters should be used. As an alternative, Eq. (28) can be used to predict slug size (diameter) when the trend of the slug frequency is available.

4.4 Model for bed expansion – larger particles

The bed expansion Δe at a fluidized state is usually defined as

$$\Delta e = \frac{H_f - H_{mf}}{H_{mf}} \tag{29}$$

where H_f is the total bed height at the fluidized state and H_{mf} is the bed height at the minimum fluidization condition. By mass balance,

$$(1 - \varepsilon_f)H_f = (1 - \varepsilon_{mf})H_{mf} \tag{30}$$

Combining Eq. (29) and Eq. (30),

$$\Delta e = \frac{1-\varepsilon_{mf}}{1-\varepsilon_f} - 1 \tag{31}$$

Applying the two-phase theory, Eq. (19) can be rearranged into

$$1 - \varepsilon_f = (1 - \delta_b)(1 - \varepsilon_{mf}) \tag{32}$$

Substituting Eq. (32) into Eq. (31), yields

$$\Delta e = \frac{1}{1-\delta_b} - 1 \tag{33}$$

From Eq. (17),

$$\delta_b = G/u_b \tag{34}$$

Combining Eq. (12) and Eq. (18),

$$G = 1.285\left(\frac{d_b}{D}\right)^{1.52} D \tag{35}$$

Substituting Eq. (22) and Eq. (35) into Eq. (34)

$$\delta_b = 0.103\left(U_0 - U_{mf}\right)^{-0.362}\left(\frac{\bar{d}_b}{D}\right) \tag{36}$$

Note that the bed expansion is over the entire bed. Hence, the bubble diameter $\bar{d}_b$ in Eq. (36) is the average value over the bed height. Substituting Eq. (36) into Eq. (33), then

$$\Delta \boldsymbol{e} = \left[\mathbf{1} - \mathbf{0.103}\left(\boldsymbol{U_0} - \boldsymbol{U_{mf}}\right)^{\mathbf{-0.362}} \left(\frac{\bar{\boldsymbol{d}}_{\boldsymbol{b}}}{\boldsymbol{D}}\right)\right]^{\mathbf{-1}} - \mathbf{1} \tag{37}$$

The explicit model given by Eq. (37) for bed expansion depends on the average bubble diameter over a bed, which is the only variable that can be linked to particle properties. The model is also applicable only in the bubbling regime, i.e. when $U_0 < U_{ms}$. To be able to predict a correct value for the bed expansion due to bubble flow, the average bubble diameter used must be dependent on the bed material properties. Most bubble diameter models available in the literature depend only on $U_0 - U_{mf}$ value, and thus provide the same results independent of the bed material. However, in Agu et al. [8], a model for average bubble diameter is proposed as described below.

$$\bar{d}_b/D = 0.848\left(\frac{U_0}{D}\right)^{0.66}\left(1 - \gamma\left(\frac{U_0}{U_{mf}}\right)^{\beta-1}\right)^{0.66}; \qquad Ar > 400 \tag{38}$$

The model parameters β and γ depend on the particle Archimedes number Ar and on the regime of flow. In addition, the expression for β depends on the particle sphericity φ. Using this bubble diameter model, a particle-dependent bed expansion model can be obtained.

Substituting Eq. (38) into Eq. (37) gives

$$\Delta \boldsymbol{e} = \left[\mathbf{1} - \mathbf{0.0873}\left(\boldsymbol{U_0} - \boldsymbol{U_{mf}}\right)^{\mathbf{-0.362}} \left(\frac{\boldsymbol{U_0}}{\boldsymbol{D}}\right)^{\mathbf{0.66}}\left(\mathbf{1} - \gamma\left(\frac{\boldsymbol{U_0}}{\boldsymbol{U_{mf}}}\right)^{\boldsymbol{\beta-1}}\right)^{\mathbf{0.66}}\right]^{\mathbf{-1}} - \mathbf{1} \tag{39}$$

The parameters, β and γ in Eq. (39) are given by

$$\beta = \varphi^{1.5}(0.329 - 1.156 \cdot 10^3 Ar^{-0.9}) \tag{40a}$$

$$\gamma = (1.321 + 8.161 \cdot 10^4 Ar^{-1.04})^{0.083} \tag{40b}$$

The result of the proposed bed expansion model, Eq. (39) is presented in Fig. 8 for sand particles with a mean diameter in the range 180 – 500 μm. The figure compares the bed expansion computed by using different models with the experimental data reported in Geldart [11]. The computations are done at the conditions used in the experiment, where $U_0 - U_{mf} = 0.06$ m/s, and the bed diameter and settled bed height are 0.3 m and 0.2 m, respectively. The minimum fluidization velocity is obtained here based on the combination of the Ergun [33] model and the Wen and Yu [34] model. Computation of minimum slugging velocity [8] shows that each particle bed is in the bubbling regime at the given gas velocity. As can be seen in Fig. 8, all the models predict the same trend as given by the experiment: the bed expansion decreases with increasing particle size. Quantitatively, the results from the model proposed in this paper agree very well with the experimental data. The slightly higher value of the bed expansion predicted by Eq. (39) is due to a higher average bubble diameter predicted from Eq. (38). The model for the average bubble diameter is developed from a deep bed where a bubble reaches its fully-grown size at a given gas velocity. It should be noted that the bed reported in [11] is shallow ($h_0/D = 0.67$). In such a shallow bed, bubble size may be smaller than in a deep bed where $h_0/D > 2$. The deviation using the Singh et al. [10] model is very high compared to other models. While the Hepbasli [9] model over predicts the experimental data, the Geldart [11] protocol under predicts the data, although the magnitude of the deviation is almost the same for both models.

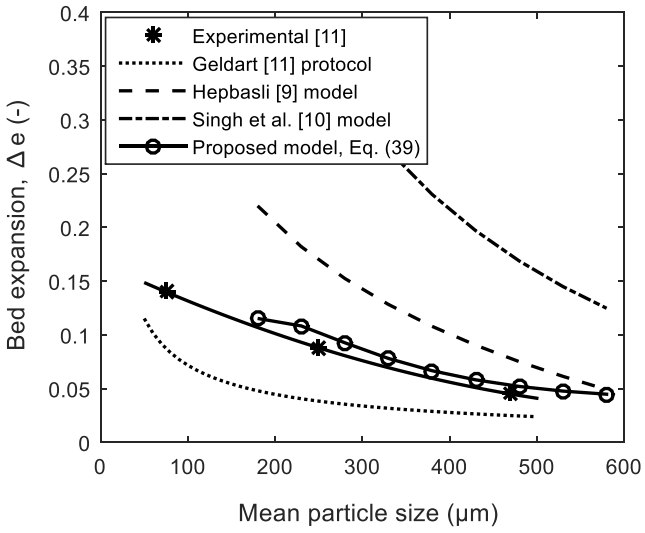

Fig. 8. Predicted bed expansion based on different models compared with the experimental data for different sand particle sizes.

Since shallow beds may contain more than one rising bubble due to lower degree of coalescence, the results in Fig. 8 show that the proposed model can also be applied for beds of multiple bubbles though a single bubble was assumed for simplicity in the development of Eq. (39). In addition to the prediction accuracy, Eq. (39) can be used at elevated temperature and pressure due to the U_0/U_{mf} term, and its dependence on the particle Archimedes number through Eq. (40). Eq. (39) also shows that the bed expansion depends on the bed diameter. Increasing the bed diameter at the same gas velocity decreases the bed expansion, which agrees with the findings in Mohanty et al. [35].

5 Conclusion

This paper presents a set of new models for predicting local bubble velocity, local bubble frequency and overall bed expansion ratio. The three models were analytically approached by considering an isolated single bubble rising in a fluidized bed. The analysis shows that bubble rise velocity is proportional to the rate of change of bubble-projected area as it passes through a fixed plane in the bed, where the proportionality constant depends on the bed diameter and

gas velocity in excess of the minimum fluidization velocity. The bed expansion model is valid in the bubbling regime and for larger particles where the particle Archimedes number is greater than 400.

The three models have been validated with experimental data obtained in this study and with some data available in the literature. The results show that the models can predict the fluidized bed properties at different gas velocities and bed diameters with good accuracy. The model for bubble velocity can predict the rise velocity of the two different types of slugs: axisymmetric and wall slugs or their mixture, accordingly. The bubble frequency model can also predict the local maximum frequency reached along the bed height or at a certain gas velocity for a given position in the bed. The dependence of the bed expansion model on the bed diameter, the fluid properties and the particle properties increases its applicability for different operating conditions, including high temperature and pressure.

6 Funding sources

This research did not receive any specific grant from funding agencies in the public, commercial, or not-for-profit sectors.

7 Reference

[1] Karimipour, S.; Pugsley, T. A Critical Evaluation of Literature Correlations for Predicting Bubble Size and Velocity in Gas-solid Fluidized Beds - A review. *Powder Technol.* **2011**, *205*, 1.

[2] Lee, S.H.; Lee, D.H.; Kim, S.D. Slug characteristics of polymer particles in a gas-solid fluidized bed. *Korean J. Chem. Eng.* **2002**, *19*, 351.

[3] Noordergraaf, I.W.; VanDijk, A.; Van Den Bleek, C.M. Fluidization and slugging in large-particle systems, *Powder Technol*. **1987**, *52*, 59.

[4] Kunii, D.; Levenspiel, O. *Fluidization Engineering*, second ed.; Butterworth – Heinemann: Washington Street, 1991.

[5] Toomey, R.D.; Johnstone, H.F. Gaseous Fluidization of Solid Particles. *Chem. Eng. Prog.* **1952**, *48*, 220.

[6] Hilligardt, K.; Werther, J. Local Bubble Gas Hold-up and Expansion of Gas/solid Fluidized Beds. *German Chem. Eng*. **1986**, *9*, 215.

[7] Grace, J.R.; Cliff, R. On the Two-phase Theory of Fluidization. *Chem. Eng. Sci*. **1974**, *29*, 327.

[8] Agu, C.E.; Pfeifer, C.; Eikeland, M.; Tokheim, L.-A.; Moldestad, B.M.E. Models for predicting average bubble diameter and volumetric bubble flux in deep fluidized beds. *Ind. Eng. Chem. Res*. **2018**, *57*, 2658.

[9] Hepbasli, A. Estimation of bed expansions in a freely-bubbling three-dimensional gas-fluidized bed. *Int. J. Energy Res*. **1998**, *22*, 1365.

[10] Singh, R.K.; Suryanarayana, A; Roy, G.K. Prediction of bed expansion ratio for gas-solid fluidization in cylindrical and non-cylindrical beds. *IE (1) Journal-CH*. **1999**, *79*, 51.

[11] Geldart D. Expansion of gas fluidized beds. *Ind. Eng. Chem. Res*. **2004**, *43*, 5802.

[12] Werther, J. Influence of the bed diameter on the hydrodynamics of gas fluidized beds. *AIChE Symp. Ser.* **1974**, *70*, 53.

[13] Choi, J.H.; Son, J.E.; Kim, S.D. Bubble Size and Frequency in Gas Fluidized Beds. *J. Chem. Eng. Jpn*. **1988**, *21*, 171.

[14] Wang, D.; Xu, M.; Marashdeh, Q.; Straiton, B.; Tong, A..; Fan, L.-S. Electrical capacitance volume tomography for characterization of gas-solid slugging fluidization with Geldart group D particles under high temperatures. *Ind. Eng. Chem. Res.* **2018,** *57,* 2687.

[15] Maurer, S.; Wagner, E.C.; Schildhauer, T.J.; Ommen, J.R.; Biollaz, S.M.A. X-ray measurements of bubble hold-up in fluidized beds with and without vertical internals. *Int. J. Multiphas. Flow* **2015**, *74*, 118.

[16] Li, X; Jaworski, A.J.; Mao, X. Bubble size and bubble rise velocity estimation by means of electrical capacitance tomography within gas-solids fluidized beds. *Measurement* **2018**, *117*, 226.

[17] Du, B.; Warsito, W.; Fan, L.-S. ECT studies of gas-solid fluidized beds of different diameters. *Ind. Eng. Chem. Res*. **2005**, *44*, 5020.

[18] Hulme, I.; Kantzas, A. Determination of bubble diameter and axial velocity for a polyethylene fluidized bed using X-ray fluoroscopy. *Powder Technol*. **2004**, *147*, 20.

[19] Davidson, J.F.; Harrison, D. *Fluidized Particles*; Cambridge University Press: London, 1963.

[20] Rowe, P.N.; Partridge, B.A. An X-ray study of bubbles in fluidized beds. *Chem. Eng. Res. Des*. **1965**, *43*, 157.

[21] Rowe, P.N.; Yacono, C.X.R. The bubbling behaviour of fine powders when fluidized. *Chem. Eng. Sci.* **1976**, *31*, 1170.

[22] Wallis, G.B. *One-dimensional two-phase flow*; McGraw-Hill: New York, 1969.

[23] Geldart, D. Types of Gas Fluidization. *Powder Technol.* **1973**, *7*, 285.

[24] Dry, R.J.; Judd, M.R.; Shingles, T. Bubble velocities in fluidized beds of fine, dense powders. *Powder Technol.* **1984**, *39*, 69.

[25] Agu, C.E.; Tokheim, L.-A.; Eikeland, M.; Moldestad, B.M.E. Determination of Onset of Bubbling and Slugging in a Fluidized Bed Using a Dual-plane Electrical Capacitance Tomography System. *Chem. Eng. J.* **2017**, *328*, 997.

[26] Werther, J. Effect of Gas Distributor on the Hydrodynamics of Gas Fluidized Beds. *Ger. Chem. Eng*. **1978**, *1*, 166.

[27] Stewart, P.S.B.; Davidson, J.F. Slug flow in fluidized beds. *Powder Technol.* **1967**, *1*, 61.

[28] Kehoe, P.W.K.; Davidson, J.F. Continuously slugging fluidized beds. *CHEMECA '70, Inst. Chem. Eng. Symp. Ser.* **1970**, *97*.

[29] Bi, X. *Flow Regime Transitions in Gas-Solid Fluidization and Transport*, Thesis; The University of British Columbia, Canada, 1994.

[30] Glicksman, L.R.; Lord, W.K.; Sakagami, M. Bubble properties in large-particle fluidized beds. *Chem. Eng. Sci*. **1987**, *42*, 479.

[31] Weber, J.M.; Mei, J.S. Bubbling fluidized bed characterization using electrical capacitance volume tomography (ECVT). *Powder Technol.* **2013**, *241*, 40.

[32] Agrawal, V.; Shinde, Y.H.; Shah, M.T.; Utikar, R.P.; Pareek, V.K.; Joshi, J.B. Estimation of bubble properties in bubbling fluidized bed using ECVT measurements. *Ind. Eng. Chem. Res*. **2018**, *57*, 8319.

[33] Ergun, S. Fluid Flow through Packed Column. *Chem. Eng. Prog*. **1952**, *48*, 89.

[34] Wen, C.Y.; Yu, Y.H. A Generalized Method for Predicting the Minimum Fluidization Velocity. *AIChE J.* **1966**, *12*, 610.

[35] Mohanty, Y.K.; Roy, G.K.; Biswal, K.C. Effect of column diameter on dynamics of gas-solid fluidized bed: A statistical approach. *Indian J. Chem. Techn*. **2009**, *16*, 17.

Nomenclature

A = cross-sectional area, m^2

Ar = dimensionless particle Archimedes number

a = instantaneous cross-sectional area, m^2

D = bed diameter, m

d = diameter, m

$\bar{d}$ = average diameter, m

Δe = dimensionless bed expansion

f = frequency, s^{-1}

G = volumetric bubble flux, m/s

g = acceleration due to gravity, m/s^2

h = vertical position in the bed from distributor, m

H = total bed height, m

k = dimensionless model coefficient

k_1 = dimensionless slug flux correction coefficient

k_2 = dimensionless wall coefficient on slug rise

m = dimensionless model coefficient

n = model parameter

r = radial position, m

t = time, s

T = period, s

U = superficial gas velocity, m/s

u_b = bubble velocity, m/s

u_{br} = single bubble rise velocity, m/s

v = volume, m^3

z = axial position, m

Greek symbols

α = dimensionless wall coefficient on bubble

β = dimensionless model parameter

δ_b = dimensionless bubble volume fraction

ε = dimensionless void fraction

$\emptyset$ = dimensionless bubble flux correction coefficient

φ = dimensionless particle sphericity

φ_D, φ_N = model coefficients

γ = dimensionless model parameter

Subscripts

b = bubble

ba = active bubble

f = fluidized

fm = maximum frequency

i = idle

mf = minimum fluidization

ms = minimum slugging

p = solid particle

0 = initial/inlet position